Improper ferroelectricity at antiferromagnetic domain walls of perovskite oxides

Yali Yang,[1,2] Hongjun Xiang,[2,3,4] Hongjian Zhao,[5] Alessandro Stroppa,[6,1] Jincang Zhang,[1,7]
Shixun Cao,[1,7] Jorge Íñiguez,[5] L. Bellaiche,[2] and Wei Ren[1,7,*]

[1]*International Centre for Quantum and Molecular Structures, Physics Department, Shanghai University, Shanghai 200444, China*
[2]*Physics Department and Institute for Nanoscience and Engineering, University of Arkansas, Fayetteville, Arkansas 72701, USA*
[3]*Department of Physics, Key Laboratory of Computational Physical Sciences (Ministry of Education),*
State Key Laboratory of Surface Physics, Fudan University, Shanghai 200433, China
[4]*Collaborative Innovation Center of Advanced Microstructures, Nanjing 210093, China*
[5]*Materials Research and Technology Department, Luxembourg Institute of Science and Technology (LIST),*
5 avenue des Hauts-Fourneaux, L-4362 Esch/Alzette, Luxembourg
[6]*CNR-SPIN, Via Vetoio, 67100 L'Aquila, Italy*
[7]*Materials Genome Institute and Shanghai Key Laboratory of High Temperature Superconductors,*
Shanghai University, Shanghai 200444, China

First-principles calculations are performed on magnetic multidomain structures in the $SmFeO_3$ rare-earth orthoferrite compound. We focus on the magnetic symmetry breaking at (001)-oriented antiphase domain walls, treating magnetism in the simplest (collinear) approximation without any relativistic (spin-orbit coupling) effects. We found that the number of FeO_2 layers inside the domains determines the electrical nature of the whole system: multidomains with odd number of layers are paraelectric, while multidomains with even number of layers possess an electric polarization aligned along b axis and a resulting multiferroic $Pmc2_1$ ground state. Our *ab initio* data and model for ferroelectricity induced by spin order reveal that this polarization is of the improper type and originates from an exchange striction mechanism that drives a polar displacement of the oxygen ions located at the magnetic domain walls. Additional calculations ratify that this effect is general among magnetic perovskites with an orthorhombic $SmFeO_3$-like structure.

I. INTRODUCTION

Multiferroic compounds have received great attention over the past years, as the coupling between ferroelectric and magnetic orderings in these materials may open promising routes for emerging electronic devices [1–3]. However, ferromagnetic and ferroelectric orders are mutually exclusive in a single compound, owing to the fact that magnetism needs non-d^0 configurations for the d electrons of transition metals, whereas ferroelectricity typically requires a d^0 configuration [4]. As a result, multiferroic materials are rather rare in nature [5], and discovering new multiferroics as well as understanding the microscopic origins for the simultaneous occurrence of their long-range ordered electric and magnetic dipoles constitute important research directions [3,6–13].

An interesting class of multiferroics is the so-called "type II" compounds in which ferroelectric order results from the symmetry breaking caused by the spin arrangement [14]. One well-known example is $TbMnO_3$, where a cycloid arrangement of the Mn spins results in an electric polarization that is strongly coupled to magnetism [15]. Recently, simpler spin arrangements in ABO_3 perovskites were found to also result in an improper ferroelectric order, provided that both A and B cationic sublattices adopt appropriate spin structures [16]. There are good reasons to believe that this is the origin of ferroelectric polarization in many rare-earth ferrites and chromites; unfortunately, the rare-earth spins generally order at very low temperatures and, hence, such multiferroism is not practical for device realizations. In this context, it is interesting to note that

$SmFeO_3$ (SFO) was reported to present ferroelectric order at much higher temperature at 670 K [17], an effect which is still unclear and under debate. No matter whether the experimental results for SFO are correct or not, they pose an interesting question, namely are there alternative mechanisms that might result in such a high-temperature polarization out of a simple highly symmetric spin lattice? Providing an answer to this question is the motivation of this paper.

Indeed, here, we would like to explore if a specific mechanism can generate an electrical polarization in SFO or, more generally, in rare-earth orthoferrites or rare-earth orthochromites sharing the same atomic structure and possessing magnetic ordering of the Fe or Cr spins. More precisely, we wish to determine if the finding recently made in double perovskite systems [18–21] can be generalized to SFO and rare-earth orthoferrites or orthochromites, with quantitative formulation of polarization arising as a result of antiferromagnetic domain antiphase boundaries. The aims of this paper are to reveal how magnetic domain boundaries can indeed generate a polarization (along a specific direction) in such compounds and to provide the microscopic features and precise driving mechanisms of such polarization, by using and analyzing first-principles simulations.

II. METHODS

All the calculations are performed within the framework of density functional theory (DFT) as implemented in the Vienna *ab initio* Simulation Package (VASP) [22]. The generalized gradient approximation (GGA) [23] in the form of the Perdew-Burke-Ernzerhof (PBE) functional and the projector augmented wave (PAW) [22] are applied to describe the

*renwei@shu.edu.cn

exchange-correlation energy and the core electrons, respectively. As mentioned in previous papers [22,24], partially filled f states are often not described well by available density functionals, and the inclusion of these $4f$ electrons leads to a problem of convergence for some physical quantities (such as noncollinear weak magnetization). Here, the $4f$ electrons of Sm^{3+} ions are kept frozen as core electrons, and 11 valence electrons for $Sm(5s^2 5p^6 5d^1 6s^2)$, $14(3p^6 3d^6 4s^2)$ for Fe and $6(2s^2 2p^4)$ for O are treated in this paper. The plane-wave cutoff is set to 550 eV. Moreover, the strong onsite Coulomb interaction on the Fe $3d$ orbitals is considered by including a Hubbard U correction [25] of 3 eV for Fe [26,27] because this value of U provides rather accurate results for a range of binary and ternary Fe oxides [28,29]. We checked that other reasonable U values yield qualitatively similar results. Note that SFO adopts the orthorhombic *Pbnm* space group [17,30,31], with the corresponding unit cell containing 20 atoms and the lattice vectors *a*, *b*, and *c* being along the $[1\bar{1}0]$, [110], and [001] pseudocubic directions [32]. In this paper, larger supercells are obtained by doubling, tripling, quadrupling, and quintupling, respectively, this 20-atom cell along the *c* axis of the *Pbnm* unit cell. The k-point grids used for integrations within the Brillouin zone (BZ) are $5 \times 5 \times 5, 5 \times 5 \times 3, 5 \times 5 \times 1, 5 \times 5 \times 1$, and $5 \times 5 \times 1$ for the resulting 20-,40-,60-,80-, and 100-atom cells, respectively. Regarding relaxations, two different cases are considered, i.e. we either choose and fix the lattice parameters of SFO to be equal to the experimental ones [32] and relax the internal atomic positions (which constitutes our Case 1) or fully relax the structures (by varying both the lattice vectors and internal atomic positions to minimize the energy, which forms our Case 2 discussed in the Supplemental Material [33]). In both cases, the Hellmann-Feynman force on each atom is converged to be less than 0.001 eV/Å. Some of the figures are drawn by the VESTA package [34].

It is important to note that, here, we present results assuming spins are perfectly collinear, i.e. without taking into account spin-orbit coupling and noncollinear magnetic effects (note that we numerically checked that, including those effects does not change qualitatively and even quantitatively some of our important results to be discussed below, such as the existence of a magnetically induced polarization in some domains). In particular, this implies that our magnetic domain walls will be very sharp, as we do not allow for the noncollinear relaxation—and spatial extension—that is typical of realistic boundaries. See Ref. [35] for a discussion of such walls in $BiFeO_3$, which is a similar compound with respect to the Fe spin order. While this is a simplification, we think our approach should be sufficient to capture the effects driven by the symmetry breaking associated with the discontinuity in the spin pattern. Beyond the most common G-type antiferromagnetic order in SFO, we also considered here other less frequent simple antiferromagnetic (A type as in $LaMnO_3$ [36] and C type as in $BiVO_3$, $BiFeO_3$, and $CaCrO_3$ [37–39]; see Fig. 1) and ferromagnetic arrangements.

III. RESULTS

Twenty-six different configurations of Fe spins are investigated. Four of them correspond to G-,C-,A-, and F-type

orders within the 20-atom *Pbnm* unit cell, and are coined G_0, C_0, A_0, F_0 in the following [see Figs. 1(a)–1(d)]. The other 22 magnetic structures are constructed by considering two antiphase boundaries of magnetic domains alternating along the *c* axis within a predominant G-,C-,A-, or F-type magnetism. As shown in Fig. 1, the spin configurations in the (001) FeO_2 layers being nearest to any domain wall have a phase change of ordering along [001] direction. Our studied magnetic domains are denoted as $Xn\text{-}m$, where $X = $ G,C,A, or F is the letter associated with the predominant magnetic ordering of each domain and where n and m represent the number of (001) FeO_2 layers in these two domains, respectively. For instance, the G2-4 structure exhibits two G-type antiferromagnetic domains having 2 and 4 (001) FeO_2 layers. Practically, the studied (n,m) combinations are (2,2), (3,3), (2,4), (4,4), (3,5), and (5,5). Some of the resulting magnetic configurations are shown in Fig. 1 with the blue and red arrows corresponding to up and down spins, respectively, and domain wall located on (001) SmO plane (indicated in green). Note that C2-2 is equivalent to G2-2 by construction, and that F2-2 is identical to A2-2. We choose the sum of n and m to be equal to an even number in order that the Sm antipolar distortions, as well as the oxygen octahedral antiferrodistortive rotational modes (as both are known to occur in the *Pbnm* state [40,41]) are compatible with the investigated supercells. As mentioned above, our considered structures are likely simpler than real magnetic domains.

Let us now concentrate on the aforementioned Case 1, when the lattice parameters are chosen to be the experimental ones. Table I shows the calculated total energies (per 5 atoms) of our 26 magnetic configurations. Here, G_0 has a lower energy than any of the three other magnetic configurations for the *Pbnm* structure with no domains (i.e., C_0, A_0, F_0) and than any of the 22 domain configurations studied here. Such a result is fully consistent with previous reports indicating that SFO has a G-type antiferromagnetic ground state [17,30,31]. We see that the total energy decreases with the domain sizes for the $Gn\text{-}m$ and $An\text{-}m$ configurations (as consistent with the concomitant decrease of domain walls' density), while the opposite holds for $Cn\text{-}m$ and $Fn\text{-}m$. This latter increase can be understood by the facts that (i) in each $Cn\text{-}m$ (respectively, $Fn\text{-}m$) structure, the Fe ions located across the antiferromagnetic domain wall experience a G-type (respectively, A-type) antiferromagnetic order which is energetically more favorable than C-type (respectively, F-type), as one can see in Table I when comparing the energies of the G_0, C_0, A_0, and F_0 structures; and (ii) Increasing the system size in $Cn\text{-}m$ (respectively, $Fn\text{-}m$) structures results in the proportion of Fe ions experiencing a G-type (A-type) spin ordering getting smaller. Similar with Ref. [42], the domain wall energies (DWEs) of the $Gn\text{-}m$ domain configurations can be calculated via $DWE = \frac{E_{Gn\text{-}m} \times (n+m)}{S_{DW}}$, where $E_{Gn\text{-}m}$ is the relative energy of the $Gn\text{-}m$ configuration with respect to G_0 (provided in Table I), and S_{DW} is the area of each domain wall in the $Gn\text{-}m$ configuration. The resulting DWEs are 0.076 J/m² for G2-2,G2-4,G3-3,G3-5, and G4-4; and 0.074 J/m² for G5-5.

To investigate if an electrical polarization can exist in our studied systems, we use the Berry Phase method [43] to compute such polarization, and also employ the FINDSYM software [44] with the tolerance 0.001 for atomic positions
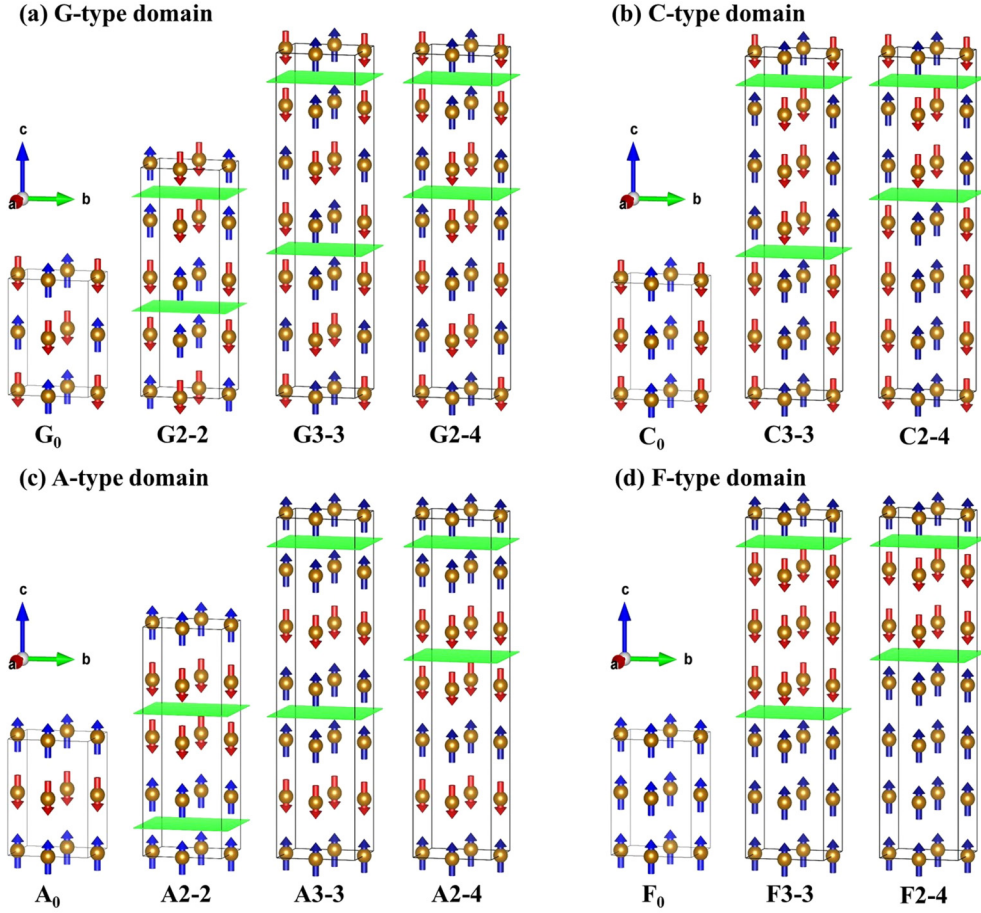
FIG. 1. Schematic of the Fe^{3+} spin arrangement in the studied X_0 magnetic monodomains and some Xn-m multidomains (see text) of SFO for (a) X = G, (b) C, (c) A, and (d) F. The green planes locate the domain walls, while blue and red arrows represent spin up and spin down, respectively.

to determine the space group of the configurations. The calculated electrical polarization values are shown in Table I. The single G_0, C_0, A_0, and F_0 domains have no polarization, as consistent with the fact that they possess the centrosymmetric

TABLE I. Calculated total energies (E, in units of eV/f.u.) and polarization (P, in units of $\mu C/cm^2$) of the Xn-m domain structures in Case 1. The energy of G_0 is set to zero. The polarizations are only along b axis with all zero along a and c axes.

Ordering	Xn-m	E	P	Ordering	Xn-m	E	P
G-type	G_0	0.000	0.000	A-type	A_0	0.172	0.000
	G2-2	0.036	-0.070		A2-2	0.217	0.069
	G3-3	0.024	0.000		A3-3	0.202	0.000
	G2-4	0.024	-0.053		A2-4	0.202	-0.047
	G4-4	0.018	-0.035		A4-4	0.194	-0.031
	G3-5	0.018	0.000		A3-5	0.194	0.000
	G5-5	0.014	0.000		A5-5	0.190	0.000
C-type	C_0	0.076	0.000	F-type	F_0	0.271	0.000
	C3-3	0.049	0.000		F3-3	0.235	0.000
	C2-4	0.049	0.053		F2-4	0.235	0.050
	C4-4	0.056	0.040		F4-4	0.244	0.039
	C3-5	0.056	0.000		F3-5	0.244	0.000
	C5-5	0.060	0.000		F5-5	0.249	0.000

$Pbnm$ space group. Similarly, all considered Xn-m configurations (with X = G,C,A, or F) for which both n and m are odd numbers are paraelectric. More precisely, the resulting ground state is found to also be $Pbnm$ when the (n,m) combinations are (3,3) and (5,5), while it becomes $P2_1/c$ when $n = 3$ and $m = 5$. On the other hand, all the investigated Xn-m configurations for which n and m are even (that is, X2-2, X2-4, and X4-4) do exhibit an electrical polarization, which is oriented parallel or antiparallel to the b axis and results in a polar $Pmc2_1$ ground state (note that two bistable $Pmc2_1$ states, having opposite directions for their polarization but the same total energy, can be generated by shifting the planes of domain walls, as illustrated in the Fig. S1. In other words, the polarization can be switched by altering the spin arrangements via domain wall motions). These polarizations range from 0.031 $\mu C/cm^2$ (for A4-4) to 0.070 $\mu C/cm^2$ (for G2-2) in magnitude (see Fig. 2), which are typical values for the polarization of so-called improper ferroelectrics [45,46] in which the polarization is induced by another physical property (e.g., spin ordering arrangements).

Analyzing the atomic displacements of the relaxed Xn-m structures with respect to their corresponding X_0 structures reveals that (1) all the ions in the Xn-m supercells can have displacements along all three directions, but with the net displacement of any type of ion (i.e., Sm, Fe, and O) along
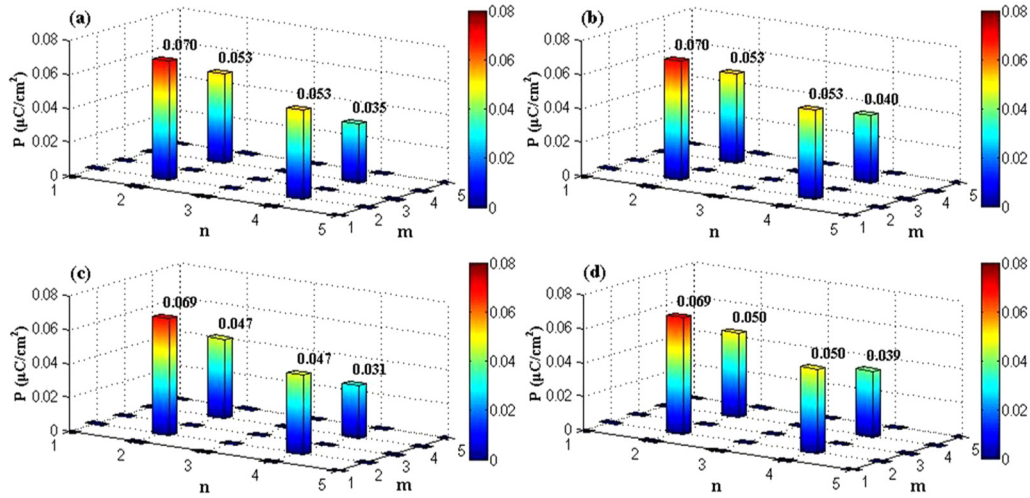
FIG. 2. Computed magnitude of the electrical polarization for the various studied combinations of n and m for Case 1 (see text) in the (a) Gn-m, (b) Cn-m, (c) An-m, and (d) Fn-m structures.

the a and c directions vanishing, when averaging over the entire supercell. This explains why there is no macroscopic polarization along the a and c axes. (2) Regarding ionic displacements along the b direction, the O ions located at the domain walls typically have much larger displacements than any other ion in the Xn-m structures. As a result, we now focus on these specific O ions and report in Fig. 3 schematization of their displacements along the b axis in the (b,c) plane for the G3-3 and G4-4 structures for Case 1. These two domains are representative of a paraelectric $Pbnm$ versus a polar $Pmc2_1$ state, respectively. In G3-3, the b component of the O is negative in one domain wall, while it is positive and has the same magnitude in the other domain wall. As a result, the net displacement along b of the O ions located at the domain walls vanishes in G3-3, which is consistent with the fact that this structure is paraelectric. On the other hand, for the G4-4 configuration, the b component of the displacement
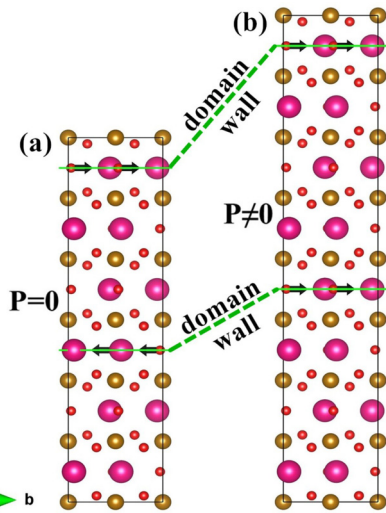

FIG. 3. Displacements of O ions (represented by black arrows) located at domain walls (represented by green lines) in the (a) G3-3 and (b) G4-4 spin configurations for Case 1 (see text).

vector of any O ion located at any domain wall is positive [see Fig. 3(b)], which therefore results in the formation of a net dipole moment along $-b$ and is thus consistent with the spontaneous polarization lying along $-b$ reported in Table I for the G4-4 domain. Such features therefore strongly suggest that the polarization numerically found in the Xn-m structures (for which both n and m are even) is related to the displacements of the O ions located at domain walls. To support this finding, we performed additional calculations on these structures, allowing only the relaxation of the O ions located at domain walls while fixing the lattice parameters to be the experimental ones and the other ions to sit at their ideal positions. Such calculations (not shown here) confirm that important results indicated in Table I can be qualitatively explained by the motions of O ions located at the domain walls. Examples of such results are the different signs of the polarization along b among our studied Xn-m structures, as well as the polarization decreasing when increasing the sum of n and m in Xn-m configurations (with n and m being even) for a given X. For instance, we numerically found that such polarization is $0, -0.241, 0, 0.161, 0.122, 0,$ and $0\,\mu\text{C/cm}^2$ for the C$_0$,C2-2 (which is also G2-2), C3-3,C2-4,C4-4,C3-5, and C5-5 structures, respectively.

Let us now check if the recently developed unified model for the spin-order induced ferroelectricity [47–50] can explain the electrical polarization induced by the magnetic domain walls in SFO as well as its microscopic origin linked to the O ions being at the domain walls. Such polarization should be due to the symmetric exchange striction mechanism $(\vec{S}_i \cdot \vec{S}_j)$ since we did not include spin-orbit coupling in our DFT calculations [51]. In this case, the spin-order-induced polarization can be written as $\vec{P} = \sum_{\langle i,j \rangle} \vec{P}_{es}^{ij} \vec{S}_i \cdot \vec{S}_j$, where the summation is over all the spin pairs $\vec{S}_i$ and $\vec{S}_j$, and $\vec{P}_{es}^{ij}$ is the polarization coefficient vector of the $\langle i,j \rangle$ spin pair. We only consider here the nearest-neighboring (NN) spin pairs for simplicity and since the magnitude of $\vec{P}_{es}^{ij}$ is typically small when the distance between $\vec{S}_i$ and $\vec{S}_j$ is large. Furthermore, since all domain walls considered in this paper
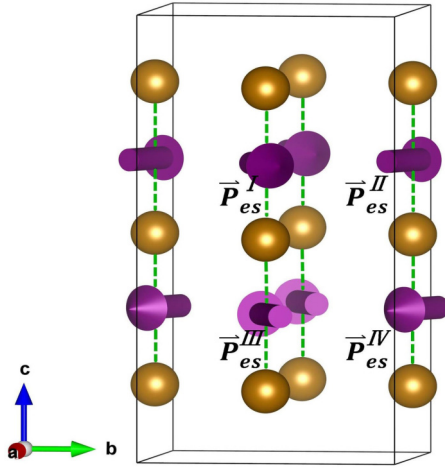
FIG. 4. Schematic illustration of the four polarization coefficient vectors $\vec{P}_{es}^{I}$, $\vec{P}_{es}^{II}$, $\vec{P}_{es}^{III}$, $\vec{P}_{es}^{IV}$ (represented by purple arrows). The brown spheres represent the Fe atoms, and the purple arrows center on the O atoms that located on SmO layer. Sm and O atoms are not shown for clarity.

are perpendicular to the c axis, only the Fe spin pairs along the c axis should contribute to the total polarization. Note also that the polarization coefficient vectors are not the same for different spin pairs, but rather are related to each other by symmetry. To be more specific and as shown in Fig. 4, there are four different polarization coefficient vectors in the *Pbnm* perovskite structure: $\vec{P}_{es}^{I} = (A, B, 0)$, $\vec{P}_{es}^{II} = (-A, B, 0)$, $\vec{P}_{es}^{III} = (-A, -B, 0)$, and $\vec{P}_{es}^{IV} = (A, -B, 0)$, where A and B are two independent parameters. Note that pairs I and II belong to the same ab plane and are located just above the pairs III and IV plane. Within this unified model, it is easy to understand (even without knowing the precise values of the A and B coefficients) why the polarization induced by the magnetic domain walls is along the b axis, without any component along the a and c axes. To illustrate this point more clearly, we take the Gn-m configurations as an example. For all the spin pairs across the magnetic domain wall along the c axis, $\vec{S}_i \cdot \vec{S}_j = 1$ (we set $|\vec{S}_i| = 1$ for simplicity) since these two spins are parallel to each other, while $\vec{S}_i \cdot \vec{S}_j = -1$ for all spin pairs being inside magnetic domains. The total polarization along the a axis will therefore cancel out since the a component of $\vec{P}_{es}^{I}$ (respectively, $\vec{P}_{es}^{III}$) is exactly opposite to that of $\vec{P}_{es}^{II}$ (respectively, $\vec{P}_{es}^{IV}$). Moreover, the polarization along the c axis also vanishes, but simply because $\vec{P}_{es}^{I}$, $\vec{P}_{es}^{II}$, $\vec{P}_{es}^{III}$, and $\vec{P}_{es}^{IV}$ all have null c components. However, the fact that the distribution of polarization coefficient vectors is periodic along the c axis with a period equal to the c lattice constant of the 20-atom *Pbnm* structure (Fig. 4) implies that a nonzero polarization can develop along the b axis in Gn-m, if the distance between two successive magnetic domain walls $d = lc$, where l is an integer. (Note that c is a lattice constant of the 20-atom orthorhombic cell, which comprises two pervoskitelike layers along that direction. Hence, $d = lc$ implies we have an even number of FeO$_2$ layers.) This is precisely what happens in

Gn-m configurations having even n and m. On the other hand, for Gn-m structures with odd n and m, the distance between two successive magnetic domain walls $d = (2l + 1)c/2$ (with l being an integer). As a result, the polarizations from these two magnetic domain walls are now in opposite direction from each other, and the resulting overall polarization vanishes in Gn-m structures with odd n and m. Note that (i) a similar argument can also explain the absence of a polarization in the single G$_0$ domain, and (ii) the existence of precisely opposite polarization at the two magnetic domains walls of the Gn-m structures having odd n and m implies that such latter configurations should be technically considered to be antipolar or antiferroelectric, while we refer to them as paraelectric in this paper.

Moreover, it is straightforward to show that the aforementioned model based on symmetric exchange striction gives a polarization $P_{Xn\text{-}m} = 8B/V_{Xn\text{-}m}$ along the b axis for Xn-m with even numbers of n and m (with $V_{Xn\text{-}m}$ being the volume of the Xn-m structure), while $P_{Xn\text{-}m} = 0$ if n and m are odd integers. Knowing that the four state mapping method [47] numerically yields $B = 2.323 \times 10^{-3}$ e$\text{\AA}$ from DFT calculations using the experimental lattice constants of SFO therefore leads to $P_{X2\text{-}2} = 0.064 \ \mu\text{C/cm}^2$, $P_{X2\text{-}4} = 2/3 P_{X2\text{-}2} = 0.043 \ \mu\text{C/cm}^2$, and $P_{X4\text{-}4} = 1/2 P_{X2\text{-}2} = 0.032 \ \mu\text{C/cm}^2$ for any $X = $ G, C, and A. These data are in rather good agreement with our DFT results of Case 1 shown in Fig. 2, which supports the validity of the model used here and thus also explains the (symmetric exchange striction) origin of the polarizations reported in Table I. Note that these types of interactions also explain why a polarization was recently found along the b axis in some double-perovskite $A_2BB'O_6$ oxides (that are systems possessing two different chemically ordered B sites) exhibiting magnetic domain walls [19–21]. Interestingly, one of the structures determined in Ref. [21] bears resemblance to our presently studied A2-2 configuration.

Such an exchange striction mechanism is also fully consistent with the idea that the polarization is related to the motion of oxygen ions being at the domain walls, since such oxygen ions are precisely located at the center of the aforementioned nonvanishing $\vec{P}_{es}^{I}$, $\vec{P}_{es}^{II}$, $\vec{P}_{es}^{III}$, and $\vec{P}_{es}^{IV}$ vectors of Fig. 4 in the case of the Xn-m configurations having a macroscopic polarization. Moreover, the significant displacement of the O ions being located at the domain walls along the $+b$ direction (see Fig. 3) makes the angle of Fe-O-Fe bonds (being initially aligned along the c axis) decreasing, which reduces the magnitude of the antiferromagnetic exchange interaction according to the Goodenough-Kanamori rule [20,52] and in turn affects the polarization coefficient vectors $\vec{P}_{es}^{ij}$ [50].

Our model further predicts a polarization of about $0.01 \ \mu\text{C/cm}^2$; that is the one reported in Ref. [17] for SFO at about 300 K, when the sum of m and n is equal to 12 or 14 (note that the G-type antiferromagnetic vector of SFO is likely not too sensitive to temperature between 300 and 0 K because of the large Neel temperature. As a result, magnetically induced polarizations should have similar value at room and low temperatures in this rare-earth orthoferrite). In other words, the polarization that we obtain might be able to explain the experimental observations of Lee *et al.* [17] provided we have a high density of magnetic domain

walls, i.e., one boundary every 12 or 14 perovskite layers. As mentioned above, our magnetic walls are narrower than those we may expect in reality, and accordingly, we can expect that our computed atomic relaxations at the walls—and associated polarizations—probably constitute an upper bound of more realistic values.

IV. SUMMARY

In summary, first-principles calculations have been performed on a variety of (initially paraelectric) Xn-m magnetic multidomains in SFO, with $X =$ G,C,A, or F being the predominant magnetic ordering existing inside each domain. These calculations allowed us to reveal that: (i) domains with even n and m integers become polar and thus multiferroic, with a polarization pointing along the b axis and of the order of 0.01–0.1 $\mu C/cm^2$, (ii) the polarization of these even n and m domains decreases as the sum of n and m increases for a given predominant magnetic ordering X, and (iii) this improper polarization is related to the motions of oxygen ions at the domain walls. Further analyzing of these first-principles calculations through the unified model for the spin-order induced ferroelectricity [47–49] demonstrates that the polarization arises from symmetric magnetic exchange striction interactions due to magnetic domain walls. In other words, it does not require spin-orbit coupling or noncollinear magnetism. Finally, we also determined the quantitative effect of relaxing the lattice vectors, in addition to the internal atomic positions, on properties of these Xn-m magnetic multidomains. For instance, such extra relaxation was found to enhance the (improper) polarization by about 73% in G2-2 and C2-2 while reducing it by about 14% in A2-2 and F2-2. We expect that this paper deepens the current knowledge of multiferroics, especially when considering that

our present results should also be generically valid for other rare-earth orthoferrites and the rare-earth orthochromite compounds that also exhibit a *Pbnm* ground state and magnetic ordering between the transition metal ions. In fact, we have performed additional calculations (not shown here) on magnetic domains in $LaFeO_3$, $GdFeO_3$, $LaCrO_3$, $NdCrO_3$, and $GdCrO_3$ materials, which do confirm such validity.

[1] J. Wang, J. B. Neaton, H. Zheng, V. Nagarajan, S. B. Ogale, B. Liu, D. Viehland, V. Vaithyanathan, D. G. Schlom, U. V. Waghmare, N. A. Spaldin, K. M. Rabe, M. Wuttig, and R. Ramesh, Science **299**, 1719 (2003).

[2] K. Aizu, Phys. Rev. B **2**, 754 (1970).

[3] H. J. Zhao, W. Ren, Y. Yang, J. Íñiguez, X. M. Chen, and L. Bellaiche, Nat. Commun. **5**, 4021 (2014).

[4] N. A. Hill, J. Phys. Chem. B **104**, 6694 (2000).

[5] N. A. Hill and A. Filippetti, J. Magn. Magn. Mater. **242**, 976 (2002).

[6] H. J. Zhao, Y. Yang, W. Ren, A.-J. Mao, X. M. Chen, and L. Bellaiche, J. Phys.: Condens. Matter **26**, 472201 (2014).

[7] P. S. Wang, W. Ren, L. Bellaiche, and H. J. Xiang, Phys. Rev. Lett. **114**, 147204 (2015).

[8] C. Xu, Y. Li, B. Xu, J. Íñiguez, W. Duan, and L. Bellaiche, Adv. Funct. Mater. **27**, 1604513 (2017).

[9] H. J. Zhao, M. N. Grisolia, Y. Yang, J. Íñiguez, M. Bibes, X. M. Chen, and L. Bellaiche, Phys. Rev. B **92**, 235133 (2015).

[10] C. J. Fennie and K. M. Rabe, Phys. Rev. Lett. **97**, 267602 (2006).

[11] A. Malashevich and D. Vanderbilt, Phys. Rev. Lett. **101**, 037210 (2008).

[12] E. Bousquet and N. Spaldin, Phys. Rev. Lett. **107**, 197603 (2011).

[13] W. Wang, J. Zhao, W. Wang, Z. Gai, N. Balke, M. Chi, H. N. Lee, W. Tian, L. Zhu, X. Cheng, D. J. Keavney, J. Yi, T. Z. Ward, P. C. Snijders, H. M. Christen, W. Wu, J. Shen, and X. Xu, Phys. Rev. Lett. **110**, 237601 (2013).

[14] D. Khomskii, Physics **2**, 20 (2009).

[15] T. Kimura, T. Goto, H. Shintani, K. Ishizaka, T. Arima, and Y. Tokura, Nature **426**, 55 (2003).

[16] H. J. Zhao, L. Bellaiche, X. M. Chen, and J. Íñiguez, Nat. Commun. **8**, 14025 (2017).

[17] J. H. Lee, Y. K. Jeong, J. H. Park, M. A. Oak, H. M. Jang, J. Y. Son, and J. F. Scott, Phys. Rev. Lett. **107**, 117201 (2011).

[18] S. Yáñez-Vilar, E. D. Mun, V. S. Zapf, B. G. Ueland, J. S. Gardner, J. D. Thompson, J. Singleton, M. Sánchez-Andújar, J. Mira, N. Biskup, M. A. Señarís-Rodríguez, and C. D. Batista, Phys. Rev. B **84**, 134427 (2011).

[19] H. Y. Zhou, H. J. Zhao, W. Q. Zhang, and X. M. Chen, Appl. Phys. Lett. **106**, 152901 (2015).

[20] J. T. Zhang, X. M. Lu, X. Q. Yang, J. L. Wang, and J. S. Zhu, Phys. Rev. B **93**, 075140 (2016).

[21] C. Y. Ma, S. Dong, P. X. Zhou, Z. Z. Du, M. F. Liu, H. M. Liu, Z. B. Yan, and J. M. Liu, Phys. Chem. Chem. Phys. **17**, 20961 (2015).

[22] G. Kresse and D. Joubert, Phys. Rev. B **59**, 1758 (1999).

[23] J. P. Perdew, K. Burke, and M. Ernzerhof, Phys. Rev. Lett. **77**, 3865 (1996).

[24] H. J. Zhao, W. Ren, Y. Yang, X. M. Chen, and L. Bellaiche, J. Phys.: Condens. Matter **25**, 466002 (2013).

[25] V. I. Anisimov, F. Aryasetiawan, and A. I. Lichtenstein, J. Phys.: Condens. Matter **9**, 767 (1997).

[26] I. V. Maznichenko, S. Ostanin, L. V. Bekenov, V. N. Antonov, I. Mertig, and A. Ernst, Phys. Rev. B **93**, 024411 (2016).

[27] T. R. Paudel, S. S. Jaswal, and E. Y. Tsymbal, Phys. Rev. B **85**, 104409 (2012).

[28] C. Ederer and N. A. Spaldin, Phys. Rev. B **71**, 060401(R) (2005).

[29] V. Stevanović, S. Lany, X. Zhang, and A. Zunger, Phys. Rev. B **85**, 115104 (2012).

[30] L. G. Marshall, J. G. Cheng, J. S. Zhou, J. B. Goodenough, J. Q. Yan, and D. G. Mandrus, Phys. Rev. B **86**, 064417 (2012).

[31] S. Cao, H. Zhao, B. Kang, J. Zhang, and W. Ren, Sci. Rep. **4**, 5960 (2014).

[32] L. Sangaletti, L. E. Depero, B. Allieri, P. Nunziante, and E. Traversa, J. Eur. Ceram. Soc. **21**, 719 (2001).

[33] See Supplemental Material at http://link.aps.org/supplemental/10.1103/PhysRevB.96.104431 for full structure relaxation, Case 2.

[34] K. Momma and F. Izumi, J. Appl. Crystallogr. **44**, 1272 (2011).

[35] Z. Gareeva, O. Diéguez, J. Íñiguez, and A. K. Zvezdin, Phys. Rev. B **91**, 060404 (R) (2015).

[36] E. O. Wollan and W. C. Koehler, Phys. Rev. **100**, 545 (1955).

[37] B. Liu, L. J. Wu, Y. Q. Zhao, L. Z. Wang, and M. Q. Cai, RSC Adv. **6**, 92473 (2016).

[38] O. Diéguez, O. E. González-Vázquez, J. C. Wojdeł, and J. Íñiguez, Phys. Rev. B **83**, 094105 (2011).

[39] A. C. Komarek, S.V. Streltsov, M. Isobe, T. Möller, M. Hoelzel, A. Senyshyn, D. Trots, M. T. Fernández-Díaz, T. Hansen, H. Gotou, T. Yagi, Y. Ueda, V. I. Anisimov, M. Grüninger, D. I. Khomskii, and M. Braden, Phys. Rev. Lett. **101**, 167204 (2008).

[40] N. A. Benedek and C. J. Fennie, J. Phys. Chem. C **117**, 13339 (2013).

[41] L. Bellaiche and J. Íñiguez, Phys. Rev. B **88**, 014104 (2013).

[42] W. Ren, Y. Yang, O. Diéguez, J. Íñiguez, N. Choudhury, and L. Bellaiche, Phys. Rev. Lett. **110**, 187601 (2013).

[43] R. D. King-Smith and D. Vanderbilt, Phys. Rev. B **47**, 1651 (1993).

[44] H. T. Stokes and D. M. Hatch, J. Appl. Crystallogr. **38**, 237 (2005).

[45] S. Picozzi and A. Stroppa, Eur. Phys. J. B **85**, 1 (2012).

[46] A. P. Levanyuk and D. G. Sannikov, Uspekhi Fizicheskikh Nauk **112**, 561 (1974).

[47] H. J. Xiang, E. J. Kan, Y. Zhang, M. H. Whangbo, and X. G. Gong, Phys. Rev. Lett. **107**, 157202 (2011).

[48] H. J. Xiang, E. J. Kan, S.-H. Wei, M. H. Whangbo, and X. G. Gong, Phys. Rev. B **84**, 224429 (2011).

[49] X. Z. Lu, M. H. Whangbo, S. Dong, X. G. Gong, and H. J. Xiang, Phys. Rev. Lett. **108**, 187204 (2012).

[50] H. J. Xiang, P. S. Wang, M. H. Whangbo, and X. G. Gong, Phys. Rev. B **88**, 054404 (2013).

[51] S. Picozzi, K. Yamauchi, B. Sanyal, I. A. Sergienko, and E. Dagotto, Phys. Rev. Lett. **99**, 227201 (2007).

[52] H. Wu, T. Burnus, Z. Hu, C. Martin, A. Maignan, J. C. Cezar, A. Tanaka, N. B. Brookes, D. I. Khomskii, and L. H. Tjeng, Phys. Rev. Lett. **102**, 026404 (2009).